Food & Function

Biological pathways via which the anthocyanin malvidin alleviated the murine colitis induced by Citrobacter rodentium

Journal:	*Food & Function*
Manuscript ID	FO-ART-09-2022-002873.R2
Article Type:	Paper
Date Submitted by the Author:	09-Dec-2022
Complete List of Authors:	Li, Robert W.; USDA-ARS Liu, Fang; Zhengzhou University Smith, Allen D.; USDA Agricultural Research Service Wang, Thomas T. Y.; USDA-ARS Beltsville Human Nutrition Research Center, Pham, Quynhchi ; USDA Agricultural Research Service Cheung, Lumei; USDA Agricultural Research Service Yang, Haiyan; Zhengzhou University

Biological pathways via which the anthocyanin malvidin alleviated the murine colitis induced by *Citrobacter rodentium*

Fang Liu[1], Allen D. Smith[2], Thomas T. Y. Wang[2], Quynhchi Pham[2], Lumei Cheung[2], Haiyan Yang[1*], Robert W. Li[3*]

[1]College of Public Health, Zhengzhou University, Zhengzhou, China

[2]USDA-ARS, Diet, Genomics, and Immunology Laboratory, Beltsville Human Nutrition Research Center, Beltsville, MD, USA

[3]USDA-ARS, Animal Parasitic Diseases Laboratory, Beltsville, MD, USA

* Correspondence:

yhy@zzu.edu.cn

Robert.Li@usda.gov

Abstract

Enteropathogenic *E. coli* (EPEC) is a causal agent for diarrheal diseases and contributes to morbidity and mortality in children under the age of five years. The emergence and rapid spread of antibiotic resistant EPEC strains necessitate the search for novel alternatives to antibiotics. In this study, we used *Citrobacter rodentium*, a natural mouse pathogen that mimics many aspects of human EPEC infections, to investigate the antimicrobial properties of the blueberry anthocyanin malvidin 3-glucoside (MG) using a multi-omics approach. MG supplementation reversed the bodyweight loss induced by *C. rodentium* infection and improved colonic hyperplasia and histopathological scores. In the colon tissue, MG supplementation significantly increased the expression of Hace1, a key regulator of TNFα-driven signaling, and impacted multiple pathways, such as TGFβ signaling. MG partially restored *C. rodentium*-induced microbial dysbiosis and significantly enhanced the abundance of the probiotic *Bifidobacterium animalis*. Moreover, MG disrupted the interactions of *E. coli* with other gut microbes. MG significantly mediated several host- and microbiota-derived metabolites, such as cytosine, ureidopropionic acid, and glutaric acid. MG normalized the bioactive lipid oleoylethanolamine, a member of the endocannabinoid system, from the dysregulated level in infected mice, directly contributing to its overall beneficial effects. Our findings provided novel insights into molecular processes via which the flavonoid malvidin exerts its biological effects in the gastrointestinal tract.

Keywords: Anthocyanin, *E. coli*, malvidin 3-glucoside, omics, tissue repair.

Introduction

Diarrheal diseases are a threat to public health and associated with a high mortality in children younger than five in developing countries [1, 2]. Enteric pathogenic *Escherichia coli* (EPEC) is considered a main causative agent inducing diarrhea [3]. Traditionally, enteric pathogenic *E. coli* have been divided into seven pathotypes, including EPEC, enterohemorrhagic *E. coli* (EHEC), enteroinvasive *E. coli* (EIEC), enterotoxigenic *E. coli* (ETEC), adherent-

invasive *E. coli* (AIEC), enteroaggregative *E. coli* (EAEC), and diffusely adherent *E. coli* (DAEC) [4]. *Citrobacter rodentium,* an *Escherichia coli*-like bacterium that naturally infects mice, shares 67% of its genes with EPEC and EHEC, including genes associated with pathogenicity and virulence [5] and causes disease in mice analogous to enteropathogenic bacterial infections in humans. In recent years, *C. rodentium* has served as a useful model to study infectious colitis [6].

EPEC, EHEC, and *C. rodentium* belong to the family of attaching and effacing (A/E) bacterial pathogens. These pathogens use an elegant Type III secretion system (T3SS) nanomachinery encoded by the locus of enterocyte effacement (LEE) to colonize the host. They process many similar characteristics and induce indistinguishable colon lesions, such as microvillus effacement, disruption of epithelial tight junctions, crypt hyperplasia, and inflammatory manifestations [7, 8]. Following oral inoculation, the gut microbiota plays a critical role in C. *rodentium* virulence gene expression and related disease progression [9]. The colon gene expression in infected mice is reprogrammed; and the expression of inflammation-related genes involved in Th1/Th17 response is significantly increased, such as, IL12, IL17, IL22, and TNFα [10]. To evade innate immune response and meet the increased cellular energetic demands, the metabolism of intestinal epithelial cells is also subverted by *C. rodentium* infection, including lipid metabolism, the tricarboxylic acid (TCA) cycle, and DNA replication pathways [11, 12].

For many years antibiotics have been widely used to control EPEC infections and reduce the mortality associated with diarrhea. However, antibiotics are not recommended for every type of diarrhea [13]. Furthermore, the emergence of antibiotic resistant *E. coli* strains and severe side effects of antibiotic use on the imbalance of intestinal microenvironment, have called for urgent actions in developing alternatives to antibiotics [14].

Natural products, such as polyphenols, with anti-inflammatory and antimicrobial properties are considered an important source of alternatives to antibiotics [15]. Malvidin 3-glucoside (MG) is one of the flavonoids responsible for the blue color in pedals of certain plants and red wine due to its high concentration in common grape vine. MG accounts for approximately 32 % of the total anthocyanin contents in blueberries and is known to possess potent antioxidative and anti-inflammatory properties [16]. MG inhibited the inflammatory response of endothelial cells via regulating NF-κB pathway [17] and increases cell viability by decreasing the level of reactive oxygen species *in vitro* [18]. Our previous study demonstrates that MG ingestion improved DSS-induced colon inflammatory responses by upregulating the

expression of IL10 *in vivo* [19]. However, the absorption rate of MG is limited [20]; and the majority of ingested MG is fermented into gallic, syringic and p-coumaric acids by gut bacteria [21]. As a result, MG exhibits a positive influence on the intestinal bacterial population and bacterial metabolism, including improving the balance of Firmicutes and Bacteroidetes, reducing the abundance of potential pathogens, such as *Clostridium perfringens,* and increasing the level of key inflammatory mediators [19, 21]. However, the effects of MG on EPEC-induced disruption on intestinal homeostasis has yet to be evaluated. We are particularly interested in understanding how MG may modulate intimate and yet reciprocal interactions between the gut microbiota and the intestinal epithelium in improving colon pathology. In this study, we attempt to evaluate the potential of the flavonoid malvidin of dietary origin as a complementary therapy for effective EPEC control using a *C. rodentium* infection mouse model.

Materials and methods

Chemical reagents

MG (CAS# 7228-78-6, MW: 528.89) was purchased from Carbosynth (Compton, UK). 10% neutral buffered formalin (Cat# HT5012), alcohol (Cat# AX0441), chloroform (Cat# 372978), isopropyl alcohol (Cat# W292907), phosphate buffered saline (Cat# P5368-5X10PAK), and methanol (Cat# 322415) were all purchased from Sigma (St Louis, MO, USA). TRIzol reagents were obtained from Thermofisher (Carlsbad, CA, USA). Lysogeny broths (LB, Cat# 1634) were supplied by ATCC. Lysing Matrix E (Cat# 6914050) was purchased from MP Biomedicals (Irvine, CA, USA). The rodent diet AIN-93M (Cat# D10012M) was purchased from Research Diets (New Brunswick, NJ, USA). ZymoBIOMICS Microbiome Standards (Cat# D6300) were purchased from Zymo Research (Irvine, CA, USA).

Citrobacter rodentium culture

A nalidixic acid-resistant *C. rodentium* strain derived from DBS100 (ATCC# 51459) was used for animal infection [22]. Briefly, a frozen stock of the primary culture was streaked out on LB agar plate; and a single colon was picked to inoculate media and incubated overnight at 37 °C with shaking at 200 rpm. The culture was expanded and grown to an OD600 value of

approximately 1.5. The bacteria were collected by centrifugation and then resuspended in media at a concentration of 1.25×10^{10} colony-forming units (cfu) per ml. The *C. rodentium* load in the colon tissue was determined by plating serial dilutions on LB agar plates with 50 μg/ml nalidixic acid for selection.

Animals and experimental protocol

All procedures regarding animal care were strictly carried out according to the animal use protocol approved by the USDA Beltsville Area Institutional Animal Care Committee (Protocol #18-027). A total of 30 C3H/HeNCr male mice at the age of five to six weeks were purchased from Charles River Laboratories (Wilmington, MA, USA). All experimental mice were fed a basal AIN-93M diet on an *ad libitum* basis and had free access to water throughout the entire experimental duration. The mean diet intake during the experiment was 0.1135 (± 0.0070) g/day/g bodyweight ($N = 30$). Two weeks after acclimatization under a 12 h light/dark cycle, the mice were randomly divided into three groups ($N = 10$ per group): Uninfected and supplemented with PBS (NC), *C. rodentium* infected and supplemented with PBS (CM), and *C. rodentium* infected and supplemented with malvidin 3-glucoside (MG). A single dose of *C. rodentium* infection at 2.5×10^9 cfu in 0.2 ml LB medium was given by oral gavage to the mice in CM and MG groups while the mice in the NC group received the equal volume of LB only. The challenge infection lasted for a total of 12 days. Five days before *C. rodentium* infection, mice in NC and CM groups received a daily dose of 0.2 ml PBS by oral gavage while the mice in the MG group received 0.2 ml MG in PBS freshly prepared daily (4 mg/kg bodyweight/day, a physiological relevant dose) via oral gavage until the end of the experiment (i.e., for a total of 17 days, including 5 days before infection and 12 after infection). Mice were monitored and weighed daily. The amount of *C. rodentium* secreted in feces was monitored by plating on the LB plate. Mice were euthanized on day 12 post-infection without fasting using the carbon dioxide asphyxiation method. The spleen tissue was aseptically removed, accurately weighed, homogenized, and plated on LB agar plates without any antibiotics to enumerate the systemic *C. rodentium* load. The length and weight of the entire colon tissue were measured. The colon contents including fecal pellets were collected, mixed and snap frozen in liquid nitrogen for metabolomics and microbiome analyses. The emptied colon was weighed and subdivided into 1-cm segments. One section was fixed in 10% neutral buffered formalin (NBF) for histology and

one snap was frozen in liquid nitrogen for total RNA extraction and subsequent RNAseq transcriptome analysis. The colon section adjacent to the anus was homogenized in LB for *C. rodentium* bacterial load determination and expressed as $\log_{10}$ cfu/g of the colon tissue.

Tissue histology

Approximately 1 cm segment of the colon tissue was fixed in 10% formaldehyde and sectioned at 5-μm thickness for hematoxylin and eosin staining (H&E). Colonic morphology and histopathological scoring were analyzed according to a previously published system [22, 23]. Tissue sections were scored for damage to the surface epithelial cells (0–4), thickness of the smooth muscle layer (0-3), crypt dilation (0-2), edema (0-2), hemorrhage (0-2), and the number of inflammatory infiltrates (0-3).

16S rRNA gene sequencing

Total DNA was extracted from colon contents using a QIAamp Fast DNA Stool Mini Kit (Qiagen) with some modifications [24]. First, a bead-beating procedure using a FastPrep 5G instrument and Lysing Matrix E was performed. Second, lysis at 70 °C was extended to 8 min. Both nuclease free water as a non-DNA template control and the microbiome standard (Zymo Research Cat# D6300; Irvine, CA, USA) were processed along with experimental samples following the same protocol and parameters to validate the entire workflow. The microbiome standard consists of three $Gram^-$ and five $Gram^+$ bacteria and two yeasts with a defined composition**.** The hypervariable V3–V4 regions of the 16S rRNA gene amplification and sequencing were performed [24]. These regions were chosen for this study due to their ability to provide a good representation of bacterial diversity in various habitats as well as their commercial availability (via the Illumina platform). The primer sequences were as follows: forward primer, 341/357F, CCTACGGGNGGCWGCAG; reverse primer, 805/785R: GACTACHVGGGTATCTAATCC. A total of 20 cycles of PCR amplification was conducted. The amplified products from individual samples were purified using AMPure XP beads (Beckman Coulter, Danvers, MA, USA). The purified PCR products were then quantified using BioAnalyzer 2100 and pooled based on an equal molar ratio and their respective samples-specific barcodes. The pooled libraries were sequenced using an Illumina MiSeq Reagent v3 Kit (Illumina).

Bioinformatic analysis of 16S rRNA gene sequences

The quality of Illumina pair-ended raw reads was checked using FastQC. The sequences with low quality score were removed using Trimmomatic. All reads were pooled using the Qiime2 tools (v2020.6) import script [25]. The dada2 in the Qiime2 pipeline was used for sequence quality control. An amplicon sequence variant (ASV) feature table was generated by the Qiime2 algorithm. Two algorithms, ALDEx2 [26], and Linear Discriminant Analysis Effect Size (LEfSe) [27], were used to detect taxa differing significantly between experimental groups. The Random Forest (RF) classification model was performed using the R package. The genus- or species-level count data derived from the ASV table were used for downstream analyses. The RF parameters used were as follows: the number of trees in the forest (ntree) was set to 501 and the number of features randomly sampled at each node in a tree (mtry) was 11. The scaled mean decrease accuracy was calculated and used to rank feature importance. Microbial association networks were constructed using a Sparse Correlations for Compositional data algorithm (SparCC v0.1.0) [28]. All raw sequence data have been deposited to the NCBI SRA database and are freely accessible (SRA accession: PRJNA877827).

Metabolomic analysis

Untargeted metabolomic analysis of colon contents was conducted as described [24]. Briefly, individual samples were accurately weighed. Methanol was added to precipitate proteins. After removing organic solvents, processed samples were characterized by an Ultra-performance liquid chromatography – tandem mass spectrometer (UPLC–MS/MS), consisting of an Acquity UPLC System (Waters, Milford, MA, USA) and a Q Exactive high resolution/accurate mass spectrometer (Thermo Scientific, Waltham, MA, USA) interfaced with a heated electrospray ionization source (ESI). Both ESI^+ and ESI^- modes were used to ionize compounds. Raw data were extracted; peaks were identified and then quantified using the area under the curve method. The raw data were aligned using Compound Discoverer (v3.1) based on the mass/charge ratio (m/z) and the retention time of the ion signals for the initial identification of metabolites. The mzMine2, an open-source software for mass-spectrometry data processing (m/z tolerance = 0.1), was used to conduct database search based on the spectra acquired. The Human Metabolome Database (HMDB) was then used for the annotation of endogenous

metabolites based on input sample types. The peak intensity data were normalized based on the median and log transformed. The normalized data were then analyzed using a hypergeometric test to identify metabolites that may differ significantly among experimental groups. The role of microbial taxa in metabolic reactions of the metabolome was derived using MetOrigin [29], an interactive bioinformatic tool that enables the origin-based metabolic pathway enrichment analysis and integrated analysis between microbiota and metabolome data relying on Sankey network visualization.

Transcriptome analysis using quantitative RT-PCR and RNAseq

Total RNA was extracted from the colon tissue using TRIzol reagents according to manufacturer's instructions. Crude total RNA was further purified using a Qiagen RNeasy Micro Kit (Qiagen, Germantown, MD, USA) with DNase digestion. RNA integrity was verified using a BioAnalyzer 2100 (Agilent, Palo Alto, CA, USA). cDNA was synthesized from total RNA using an iScript Advanced cDNA Synthesis Kit (Biorad, Hercules, CA, USA). Quantitative RT-PCR reactions were carried out using a CFX Connect Real-Time PCR Detection System (BioRad). The reactions were run in duplicates in a total volume of 20 µl containing the following: 2 µl of cDNA (100 ng), 0.5 µl of each primer (forward and reverse, 20 nM each), 11 µl of SsoAdvanced Universal SYBR Green Supermix and 6 µl of nuclease-free water. The amplification reactions were subjected to an initial denaturation at 95 °C for 3 min, followed by 40 cycles of 95 °C for 30 s, 60 °C for 30 s, and 72 °C for 30 s. A standard-curve based absolute quantification method was used.

RNAseq libraries were prepared using an Illumina TruSeq RNA sample prep kit following the manufacturer's instructions (Illumina). The libraries for each sample were pooled at an equal molar ratio and based on their respective sample-specific barcodes. Paired-end sequences were generated at 150 bp/read using an Illumina NovaSeq sequencer. The quality of raw sequences was checked using FastQC (v0.11.9). Raw sequences were then trimmed using Trimmomatic (v0.38). The preprocessed reads were analyzed using STAR-DESeq2 (v1.31.16) pipeline [30] with default parameters. False discovery rate (FDR) < 0.05 was used as a cutoff for determining differentially expressed genes. Gene enrichment analysis was conducted using gene set enrichment analysis (GSEA, v4.2.3) [31]. GSEA was performed with following parameters: The number of permutations = 1000, minimum term size = 15, and maximum term size = 500.

Statistical analysis

Statistical analyses were performed using the R Stats package (R version 4.3.0). The two-group comparison was made using the non-parametric Wilcoxon Rank Sum (Mann–Whitney U test) while the Kruskal–Wallis test by rank (KW) were used for multi-group comparisons. The number was expressed as means ± SD, unless stated otherwise in the main text, figure legends or supplementary tables. The p value ≤ 0.05 was considered statistically significant. For untargeted metabolome data, FDR corrections were applied to unadjusted p values generated using the Wilcoxon Rank-Sum test, whereby statistical significance was considered at FDR-adjusted q values ≤ 0.05. For pathway enrichment analysis, Fishers' exact test was used to identify if a pathway is enriched or perturbed, as opposed to by random chance. In this case, only the number of hits, i.e., the number of metabolites or genes that match to a particular pathway was computed. For RNAseq based transcriptome analysis, the standard DESeq 2 algorithm was used; and significance threshold was also considered at FDR-adjusted q values ≤ 0.05. For 16S rRNA gene-based microbiome data, differentially abundant taxon identification was performed using LEfSe and ALDEx2. The former uses KW to detect taxa with significant differential abundance between treatment groups and linear discriminant analysis (LDA) to estimate the effect size of each differentially abundant taxon with the absolute LDA value ≥ 2.0 as a cutoff. ALDEx2 uses the centered log-ratio transformation to deal with the compositional data issue inherent in marker gene count tables. It outputs multiple adjusted p values, including Benjamini-Hochberg corrected p value from Wilcoxon rank sum tests. ALDex2 is not sensitive to data characteristics but sometimes tends to underestimate the true FDR. As a result, the findings from LEfSe were discussed in detail in the main text.

Results

Malvidin intervention improved colon pathology induced by Citrobacter rodentium infection in mice

Compared with uninfected healthy mice with a mean bodyweight gain of 1.2 ± 0.6 g during the experimental duration, the mice infected by *C. rodentium* experienced a bodyweight

loss of 0.6 ± 0.8 g during the same period (Fig. 1A). MG supplementation significantly increased the bodyweight by 0.3 g ($p < 0.01$) during the period. However, the colon C. *rodentium* bacterial load ($\log_{10}$ cfu/g) at 12 days post-infection remained unchanged by MG supplementation (Fig. 1B), suggesting that the positive effect of MG on mouse bodyweight gain may not be correlated with colon colonization by *C. rodentium*. Furthermore, while both colon weight (Fig. S1A, Supplementary file) and the spleen index (the ratio of spleen weight to the bodyweight, Fig. S1B) increased in response to *C. rodentium* infection, MG supplementation seemingly had little effect on both parameters. Intriguingly, MG supplementation significantly shortened the crypt length ($p < 0.05$, Fig. 1C). The colon crypt length was significantly increased by *C. rodentium* infection from 144.69 ± 19.11 μm in uninfected control mice to 353.18 ± 37.75 μm ($p < 0.001$). The colon pathology induced by *C. rodentium* infection was affected by MG intervention (Fig. 1D), as reflected on various colon histopathological scores, including the thickness of the colon muscle layer, hemorrhage, the number of inflammatory infiltrates, and crypt dilation (Fig. S2).

Malvidin modulated inflammatory signaling pathways in the colon tissue in response to Citrobacter rodentium infection

To determine the biological pathways through which MG improved *C. rodentium*-induced pathology, the colon transcriptome was characterized using RNAseq and related bioinformatics analysis. *C. rodentium* infection had a profound impact on colon gene expression and resulted in a significant alteration to the colon transcriptome, including 5,102 upregulated genes and 6,238 downregulated genes at a combined cutoff threshold of FDR of 5% and absolute fold change (FC) > 2.0, compared to in uninfected control mice (Fig. S3A). Gene set enrichment analysis (GSEA) was performed to identify the pathways significantly enriched at stringent cutoff thresholds (the absolute normalized enrichment score value (NES) >1 and adjusted $p < 0.05$). The GSEA analysis identified multiple inflammatory pathways that were highly enriched in *C. rodentium* infected mice, including TNFα signaling via NF-κB (NES = 2.48, p and q = 0.0000; Fig. S3B), IL6-JAK-STAT3 signaling (NES = 2.58, p and q = 0.0000; Fig. S3C), interferon gamma response (NES = 3.21, p and q = 0.0000; Fig. S3D) and inflammatory response (NES = 2.32, p and q = 0.0000; Fig. S3E). Furthermore, the Wnt β-catenin signaling pathway, known to be involved in intestinal epithelia repair and renewal [32], was negatively regulated by *C. rodentium* infection (NES = -1.41, $p = 0.0446$, and q = 0.0419; Fig. S3F).

MG supplementation in mice infected with *C. rodentium* significantly affected the expression of 12 genes in the colon tissue, including 7 upregulated genes and 5 downregulated genes (Fig. 2A), such as Tchh, a gene encoding trichohyalin. At the pathway level, as detected by GSEA, MG supplementation significantly modulated the TGFβ signaling pathway (Fig. 2B; NES = -1.49, $p = 0.0196$, and FDR = 0.0359). Moreover, TNFα signaling via NF-κB pathway, which was highly enriched by *C. rodentium* infection, was also significantly enriched by MG supplementation (Fig. 2C). Interestingly, a gene encoding HECT domain E3 ligase 1 (Hace1), which acts as a tumor suppressor and regulator of TNFα-driven NF-κB, was significantly upregulated by MG. The expression level of Hace1 in the colon tissue in the MG group was significantly higher than in the CM group ($p < 0.01$; Fig. 2D). Further, among the genes downregulated by *C. rodentium* infection, MG supplementation reversed the expression of multiple genes to the basal line levels, such as Lmbr1 domain containing 2, Lmbred2 ($p <0.001$; Fig. 2E) and ADP-ribosylation factor-like 13B, Arl13b ($p <0.001$; Fig. 2F).

Malvidin supplementation significantly increased the abundance of probiotic species and promoted gut microbial interactions

C. rodentium infection had a profound impact on gut microbial composition and microbial diversity. Beta-diversity analysis using constrained principal coordinate analysis (CPCoA) based on Bray-Curtis dissimilarity revealed a clear separation in the gut microbial community among the three groups, uninfected control mice supplemented with PBS for 17 days (NC), mice infected by *C. rodentium* supplemented with either PBS (CM) or with MG (Fig. 3A) for 17 days. Furthermore, *C. rodentium* infection significantly altered the abundance of at least four phyla, such as Firmicutes, Proteobacteria, TM7, and Tenericutes (linear discriminant analysis LDA scores >2.0 and $p < 0.05$; Fig. 3B). The relative abundance of Proteobacteria was significantly increased by *C. rodentium*, from 2.57% in uninfected mice to 8.70% in infected mice, while the abundance of Firmicutes, TM7, and Mycoplasmatota (originally named Tenericutes) was significantly decreased by *C. rodentium* induction (Fig. 3B). However, at the phylum level, MG supplementation did not significantly reverse the changes induced by *C. rodentium* (data not shown).

At the species level, the abundance of multiple potentially opportunistic pathogens was significantly increased by *C. rodentium* infection, as compared to uninfected control mice (Table

S1), such as *Alistipes finegoldii*, *Lactobacillus vaginalis*, *Clostridium glycolicum*, *Clostridium cocleatum*, and *E. coli*. Both *A. finegoldii* and *C. glycolicum* were undetectable in the uninfected control mice but their abundance was significantly increased by *C. rodentium*. Moreover, the abundance of butyrate-producing species, *Butyricicoccus pullicaecorum,* was significantly decreased by *C. rodentium* from 0.09% in uninfected mice to 0.02% in infected mice (LDA score > 2.0, $p < 0.05$; Table S1). Further, MG supplementation resulted in a marginal decrease in the abundance of pathogenic species, including *A. finegoldii*, *L. vaginalis*, *C. cocleatum*, *C. glycolicum,* and *E. coli*. Among them, MG supplementation reduced the abundance of *E. coli* by > 5 fold ($p = 0.09$), suggesting that MG may indeed possess antimicrobial property *in vivo*. Interestingly, MG ingestion significantly increased the abundance of *Bifidobacterium animalis,* a species with probiotic potential (LDA > 3; $p < 0.05$; Fig. 3C). A machine learning algorithm, Random Forests (RF), ranked 15 most important species that enabled an accuracy classification between the groups with or without MG supplementation (Fig. 3D). Notably, RF classification model ranked *B. animalis* among the most important species in classifying the MG intervention based on mean decrease accuracy.

The microbial association networks in fecal microbial communities of mice in the three treatment groups, NC, CM, and MG, were constructed at a species level derived from the ASV table using SparCC. The significant correlations ($p < 0.05$) between gut bacterial species are shown in Fig. 4. The results indicated that *C. rodentium* infection and MG supplementation significantly modulated microbial interactions, especially for those opportunistic pathogens present in the gut microbial community. For examples, in the CM interaction network, *C. cocleatum* was positively correlated with *Bacteroides acidifaciens* (r = 0.7550), *Parabacteroides* (r = 0.9177), *A. finegoldii* (r = 0.8260), Lachnospiraceae (r = 0.6805), Peptostreptococcaceae (r = 0.6725), and *Coprobacillus* (r = 0.6739). MG supplementation disrupted the microbial interaction of *C. cocleatum* observed in the infected mice supplemented with PBS. In the network of MG supplemented mice, *C. cocleatum* was positively correlated with *Lactobacillus* (r = 0.7928), *Streptococcus* (r = 0.6578), *L. vaginali* (r = 0.6263) and *Anaerotruncus* (r = 0.7974) but was negatively correlated with *Bilophila* (r = -0.8015) ($p < 0.05$). Notably, MG also modulated the species interactions of *E. coli* in infected mice. As Fig. 4 shown, *E. coli* was positively correlated with 5 nodes (such as *C. glycolicum*) and was negatively correlated with 4 nodes (such as Clostridiales) in the CM network ($p < 0.05$). MG supplementation completely

disrupted the microbial interactions; and no nodes were significantly correlated with *E. coli* in the MG network, having reversed to the baseline level observed in the NC network. Further, MG supplementation promoted microbial interactions between *B. animalis* and other gut microbes, which displayed positive correlations with *S24-7* (r = 0.5372), *Dehalobacterium* (r = 0.5512), and *Sutterella* (r = 0.5742).

Alterations in the fecal metabolome induced by Citrobacter rodentium infection and their relevance to the gut microbiota

Untargeted metabolome analysis detected and annotated at least 513 metabolites in feces, including 12 metabolites derived from the host, 55 metabolites of microbiota origin, 164 metabolites from both the host and microbiota, and 282 metabolites of exogenous or dietary origin (Fig. S4). *C. rodentium* infection resulted in a significant alteration in global metabolite profiles. 14 metabolites were significantly downregulated while 37 metabolites were upregulated by *C. rodentium* infection ($p < 0.05$; Table S2). For example, serotonin, which is derived from either the host or the microbiota (Co-metabolism), was increased 2.48-fold by infection, compared to the uninfected control group (Table S2; Fig. 5A). Additionally, *C. rodentium* infection led to 2.30-fold and 4.49-fold decreases in ureidopropionic acid and indoleacetaldehyde, respectively. The metabolites significantly altered by infection were enriched in multiply pathways ($p < 0.05$, Fig. 5A), such as host-derived beta-alanine metabolism pathway, microbiota-derived pyrimidine metabolism and prodigiosin biosynthesis pathways, and tryptophan metabolism, sphingolipid metabolism, D-alanine metabolism, primary bile acid biosynthesis and steroid biosynthesis pathways of mixed origin (Co-metabolism).

The correlations between fecal metabolites and microbial taxa were also analyzed using the MetOrigin algorithm (Fig. 5B). At a genus level, *Escherichia,* its abundance was elevated by infection, was positively correlated with indolelactic acid, a key metabolite in tryptophan metabolism pathway, and negatively correlated with cytosine and cytidine in pyrimidine metabolism pathway ($p < 0.05$; Fig. 5B). The abundance of *Coprococcus*, which was decreased by *C. rodentium* infection, was negatively correlated with indolelactic acid ($p < 0.05$), in contrast to *Escherichia*. At a species level, *C. rodentium* and indoleacetaldehyde showed a significantly negative correlation while *E. coli* displayed a significantly positive correlation with indolelactic acid in the metabolic reaction R02678 (Fig. 5C), part of tryptophan metabolism. Additionally,

the content of serotonin was positive related with several bacterial species, such as *L. vaginalis* and *E. coli*, in the metabolic reaction of R02908 ($p < 0.05$; Fig. 5D), also part of tryptophan metabolism.

MG supplementation affected approximately 5% of all metabolites detected in feces, MG intake reduced the level of 15 metabolites and increased that of 8 metabolites, compared to infected mice supplemented with PBS (Fig. 6A). The level of multiple metabolites, such as ureidopropionic acid and SM (d18:1/16:0), both being microbiota–host co-metabolites, 2(R)-hydroxydocosanoic acid and oleoylethanolamine (OEA) (food origin), and cytosine (a microbiota-derived metabolite), was significantly reversed by MG supplementation from the elevated level in the infected group ($p < 0.05$; Table S2). Moreover, MG supplementation resulted in a significantly lower concentration of glutaric acid, indole, and pantothenic acid by 2.7-fold, 5.5-fold, and 3.2-fold, respectively, compared to the infected group ($p < 0.05$; Fig. 6B). These metabolites were significantly enriched in 12 pathways, such as beta-Alanine metabolism, pantothenate and CoA biosynthesis, pyrimidine metabolism pathways, microbiota-derived phenylalanine, tyrosine and tryptophan biosynthesis, lysine degradation and tryptophan metabolism pathways (Fig. 6C; $p < 0.05$). To understand potential roles of gut microbes in certain metabolic reactions, an integrated analysis between biological knowledge and statistical correlations was conducted using powerful Sankey network tool in the MetOrigin algorithm. The "Microbiota" network suggested that two metabolites significantly downregulated by MG were positively associated with the genera *Escherichia* and *Streptococcus* (Fig. 6D). Further, in the "Co-metabolism" network, three significantly disregulated metabolites were also correlated with these two genera (Fig. 6D). At a species level, the level of indole was positively associated with *C. glycolicum* in the metabolic reaction R00673, which belongs to tryptophan metabolism pathway (Fig. 6E).

Discussion

Numerous studies have demonstrated that anthocyanins in common fruits possess antioxidative, antimicrobial, and anti-inflammatory properties and can be considered potential alternative to antibiotics [33]. The total anthocyanin content in fresh whole blueberries and blueberry skins can reach 0.22% and 1.77%, respectively [34]. As a dominant anthocyanin,

malvidin accounts for up to 32% of the total anthocyanins in blueberries, depending on cultivars and growing conditions. In addition to being used as a common food colorant, the health benefit of malvidin has been recently recognized. As a potent antioxidant, malvidin can significantly reduce cellular free radicals and, subsequently, the risk of cardiovascular conditions [35]. Further, its anti-inflammatory and microbiota-modulating activities have also been investigated [19]. In vitro studies show that blueberry extracts possess antibacterial properties. *Citrobacter freundii* and *Enterococcus faecalis* are among the bacterial species most sensitive to these extracts [34]. The extrapolation of the findings from rodent studies suggests that a daily intake of approximately 200 mg malvidin, in the form of malvidin-rich beverage, food products or fruits, can significantly ameliorate intestinal inflammation and restore altered gut microbial composition in humans [19].

In recent years, antibiotic resistant EPEC strains have become highly epidemic pathogens in communities and hospitals [36]. EPEC can attach to host cell membrane via outer membrane protein-intimin interactions, leading to a disruption of the cell surface and subsequent delivery of effector proteins into host intestinal cells [37]. The consequence of successful EPEC attachment and invasion is the imbalance of the immune responses and loss of cellular function. As a result, minimizing the attachment of EPEC and regulating EPEC-gut microbiota interactions may represent several key points of effective intervention in diminishing EPEC induced pathology. While MG resulted in a 5-fold reduction in the abundance of *E. coli*, our *in vivo* findings did not provide strong evidence that MG was bactericidal to *C. rodentium* in intestinal epithelial surface. Subsequent studies are warranted to validate these findings using different animal models and MG delivery routes. Nevertheless, colon pathology, particularly crypt hyperplasia and gross histology scores, was significantly improved by MG supplementation.

It is well known that during the infection, multiple innate and adaptive immune signaling pathways, such as NF-κB signaling and IL22 signaling, and interferon regulatory factors, are provoked to prevent the establishment of *C. rodentium* and eliminate its invasion [38]. Our findings demonstrated that MG supplementation resulted in a perturbation of TNFα signaling via NF-κB. Previous studies show that NF-κB-mediated TNFα promotes antimicrobial immunity and plays a critical role in pathogen clearance [39]. TNFα-NF-κB-dependent pathogen clearance is regulated by Hace1[40], a tumor suppressor [41] that plays a positive role in promoting pathogen clearance and inhibiting intestinal inflammation [40]. Our results show that MG was able to significantly

upregulate the expression of Hace1 in the colon tissue from the depressed level induced by *C. rodentium* (Fig. 2D). Moreover, MG significantly impacted TGFβ signaling pathway, which was downregulated by infection [42]. The suppression of TGFβ signaling pathway is known to be associated with inflammation and contribute to colon pathogenesis [43, 44]. Inversely, the activation of TGFβ signaling pathway is beneficial to tissue repair [45]. Together, our findings provided evidence that MG intake improved the colon lesion induced by infection likely via the activation of the pathways involved in tissue repair and the regulation of intestinal inflammation.

One of the promising alternative EPEC control strategies entails modulating the gut microbiota, which warrants continued evaluation of the antimicrobial properties of natural products, including flavonoids of common fruits. Our data provided additional evidence that *C. rodentium* infection severely disrupts the structure and composition of the gut microbiota, including a significant increase in the abundance of Proteobacteria (Fig. 3), in agreement with published reports [46]. During *C. rodentium* infection, intestinal microbiota plays a crucial role in regulating mucosal inflammatory responses and restoring epithelial barrier function [6]. Previous studies also indicate that the decreased abundance of commensal species with probiotic potential, such as *Lactobacillus,* may be important for colitis pathogenesis [46]. MG, which can be metabolized by gut microbes, stimulates the growth of species assigned to *Bifidobacterium* and *Lactobacillus* [47]. In our study, MG supplementation protected against *C. rodentium*-induced microbial disruptions. The abundance of *B. animalis* was significantly increased due to MG intake. As one of the major probiotics, *B. animalis* is known to have a protective effect on intestinal health in both clinical trial and animal models. In a clinical trial with infants, *B. animalis* supplementation resulted in a significant increase in immune regulators and antibacterial molecules, such as sIgA, butyrate, cathelicidin, and beta-defensin-2 (HBD-2), leading to a significant improvement in stool consistency [48]. In DSS-induced colitis mice, the expression of tight junction proteins was significantly increased whereas TLR4/MYD88/NF-κB signaling pathway was inhibited by *B. animalis* supplementation [49]. Furthermore, *B. animalis* increases the secretion levels of TGFβ in patients with ulcerative colitis [50]. Our data in *C. rodentium* model established a negative correlation between the abundance of *B. animalis* and that of *C. cocleatum*, a potential human pathogen. MG supplementation was also associated with a 46% reduction in the abundance of *Ruminococcus gnavus,* a pathogenic species, validating the findings using a chemical induced colitis model [19]. Together, these data suggest that malvidin-

induced increase in the probiotic *B. animalis* likely contributed to overall health benefits of anthocyanin-rich fruits and that interventions by the synbiotics consisting of malvidin and *Bifidobacterium* species may be complementary to classical antibiotic controls of EPEC infections.

Furthermore, MG seemingly promoted microbial species interactions in the gut microbial community in the *C. rodentium* infected mice (Fig. 4). *E. coli*, one of the opportunistic human pathogens, was inhibited about 5-fold by MG in these mice, suggesting that MG likely possesses antimicrobial properties. The overgrowth and invasion of specific *E. coli* strains had been considered an important factor for inflammatory bowel disease (IBD) relapse [51]. In uninfected control mice, no other bacterial species were strongly associated with *E. coli*. However, in the *C. rodentium* infected mice without MG supplementation, *E. coli* was strongly associated with several other several pathogens, including *C. glycolicum* and species from the family Enterobacteriaceae. MG supplementation completely disrupted such associations. These findings provided additional support to the notion that MG intake may be associated with the reduced risk of pathogen infections.

In this study, at least 513 fecal metabolites were positively identified and annotated. The origin of these metabolites is broad-based, included host-derived and microbiota-derived metabolites, in addition to metabolites of both host and microbiota origin and endogenous or dietary origin. *C. rodentium* infection resulted in approximately 10% of the total metabolites to be dysregulated. Among these, MG supplementation reversed the trends for at least five metabolites. Intriguingly, MG normalized the amount of OEA in the gut contents from an elevated level in the infected mice (54% reduction, $p = 0.024$). As a member of the endocannabinoid system, a metabolic pathway involved in the communication between the gut microbiota and the host [52], OEA is known to act as a peroxisome proliferator-activated receptor type-α agonist [53]. OEA suppresses appetite by stimulating satiety in mice [54]. Our findings that MG associated reduction in OEA levels may partially explain the restoration of the infection-induced bodyweight loss resulting from MG intake. The findings from a small randomized, double-blind, placebo-controlled clinical trial with obese individuals demonstrates that an eight-week OEA intervention resulted in a significant decrease in serum IL6 and TNFα concentrations [55], suggesting that OEA may have therapeutic value. OEA is synthesized from dietary oleic acid in enterocytes. Recent studies demonstrated that OEA treatment decreases body weight and food

consumption [56]. OEA treatment alters the ratio of Firmicutes to Bacteroidetes. In this study, OEA was positively correlated with the abundance of *Streptococcus* (r = 0.62; $p = 0.04$), which harbors non-pathogenic commensal species in humans. While the statistical association does not indicate causality, the positive correlations between OEA and microbial taxa warrant further investigations. The recent evidence demonstrates that approximately one third of the anti-inflammatory effect of short-chain fatty acids (SCFA) are mediated by endocannabinoids (EC), including OEA, in healthy individuals with or without exercise [57]. At baseline, all four EC tested, OEA, as well as 2-arachidonoylglycerol (2-AG), anandamide (AEA), and N-palmitoylethanolamine (PEA), are positively associated with alpha diversity, such as Shannon index, and SCFA-producing bacteria. Circulating OEA, which is significantly increased by exercise, is also positively correlated with both serum SCFA and IL10 levels ($P < 0.05$) but negatively correlated with proinflammatory cytokines, such as TNFa and IL6 (Vijay et 2021). OEA and other EC have been suggested to act as a regulator of the intestinal barrier integrity [52] and affect the permeability of enterocytes [58]. Together, we hypothesize that MG likely acted as an inhibitor of N-acyl phosphatidylethanolamine-specific phospholipase D, a key enzyme in OEA biosynthesis pathway [53]. Indeed, deletion of the gene encoding this enzyme reduces OEA levels [59]. Our future work will test this hypothesis using *in vitro* and *in vivo* models and unravel possible its mechanisms of action.

In conclusion, malvidin from dietary sources can act as a key regulator of the signaling pathways related to intestinal inflammation and tissue repair in a mouse model. As a possible antimicrobial alternative, malvidin promotes the probiotic *Bifidobacterium animalis* and disrupts the microbial association between *E. coli* and other gut microbes. Malvidin regulates an important bioactive lipid in the endocannabinoid system and may mediate the anti-inflammatory properties of gut metabolites produced via microbial fermentation.

Availability of data and materials

Raw sequences data have been deposited at the NCBI SRA database and are publicly available. The accession number is PRJNA877827. Any additional information required to reanalyze the data reported in this paper, such as raw spectrum data, is available from the lead

contact upon request.

Acknowledgements

Mention of trade names or commercial products in this publication is solely for the purpose of providing specific information and does not imply recommendation or endorsement by the U. S. Department of Agriculture (USDA). The USDA is an equal opportunity provider and employer.

Author contributions

FL, HY, and RWL conceived the study and designed the experiment. FL, ADS, TTYW, QP, and LC performed the experiment. FL analyzed the data. FL, HY, and RWL drafted the manuscript. All authors approved the manuscript.

Conflict of Interest

Authors declare no conflicts of interest.

References

1. T. Nhampossa, I. Mandomando, S. Acacio, L. Quinto, D. Vubil, J. Ruiz, D. Nhalungo, C. Sacoor, A. Nhabanga, A. Nhacolo, P. Aide, S. Machevo, B. Sigauque, A. Nhama, K. Kotloff, T. Farag, D. Nasrin, Q. Bassat, E. Macete, M. M. Levine and P. Alonso, Diarrheal Disease in Rural Mozambique: Burden, Risk Factors and Etiology of Diarrheal Disease among Children Aged 0-59 Months Seeking Care at Health Facilities, *PLoS One*, 2015, **10**, e0119824.
2. S. Shine, S. Muhamud, S. Adanew, A. Demelash and M. Abate, Prevalence and associated factors of diarrhea among under-five children in Debre Berhan town, Ethiopia 2018: a cross sectional study, *BMC Infect Dis*, 2020, **20**, 174.
3. B. Pakbin, W. M. Bruck and J. W. A. Rossen, Virulence Factors of Enteric Pathogenic Escherichia coli: A Review, *Int J Mol Sci*, 2021, **22**.
4. A. Clements, J. C. Young, N. Constantinou and G. Frankel, Infection strategies of enteric pathogenic Escherichia coli, *Gut Microbes*, 2012, **3**, 71-87.
5. N. K. Petty, R. Bulgin, V. F. Crepin, A. M. Cerdeno-Tarraga, G. N. Schroeder, M. A. Quail, N. Lennard, C. Corton, A. Barron, L. Clark, A. L. Toribio, J. Parkhill, G. Dougan, G. Frankel and N. R. Thomson, The Citrobacter rodentium genome sequence reveals convergent evolution with human pathogenic Escherichia coli, *J Bacteriol*, 2010, **192**, 525-538.
6. J. W. Collins, K. M. Keeney, V. F. Crepin, V. A. Rathinam, K. A. Fitzgerald, B. B. Finlay and G. Frankel, Citrobacter rodentium: infection, inflammation and the microbiota, *Nat Rev Microbiol*, 2014, **12**, 612-623.
7. X. Xia, Y. Liu, A. Hodgson, D. Xu, W. Guo, H. Yu, W. She, C. Zhou, L. Lan, K. Fu, B. A. Vallance and F. Wan, EspF is crucial for Citrobacter rodentium-induced tight junction disruption and lethality in immunocompromised animals, *PLoS Pathog*, 2019, **15**, e1007898.
8. A. R. Wong, J. S. Pearson, M. D. Bright, D. Munera, K. S. Robinson, S. F. Lee, G. Frankel and E. L. Hartland, Enteropathogenic and enterohaemorrhagic Escherichia coli: even more subversive elements, *Mol*

Microbiol, 2011, **80**, 1420-1438.
9. C. Mullineaux-Sanders, J. W. Collins, D. Ruano-Gallego, M. Levy, M. Pevsner-Fischer, I. T. Glegola-Madejska, A. M. Sagfors, J. L. C. Wong, E. Elinav, V. F. Crepin and G. Frankel, Citrobacter rodentium Relies on Commensals for Colonization of the Colonic Mucosa, *Cell Rep*, 2017, **21**, 3381-3389.
10. Y. Zheng, P. A. Valdez, D. M. Danilenko, Y. Hu, S. M. Sa, Q. Gong, A. R. Abbas, Z. Modrusan, N. Ghilardi, F. J. de Sauvage and W. Ouyang, Interleukin-22 mediates early host defense against attaching and effacing bacterial pathogens, *Nat Med*, 2008, **14**, 282-289.
11. C. N. Berger, V. F. Crepin, T. I. Roumeliotis, J. C. Wright, N. Serafini, M. Pevsner-Fischer, L. Yu, E. Elinav, J. P. Di Santo, J. S. Choudhary and G. Frankel, The Citrobacter rodentium type III secretion system effector EspO affects mucosal damage repair and antimicrobial responses, *PLoS Pathog*, 2018, **14**, e1007406.
12. C. N. Berger, V. F. Crepin, T. I. Roumeliotis, J. C. Wright, D. Carson, M. Pevsner-Fischer, R. C. D. Furniss, G. Dougan, M. Dori-Bachash, L. Yu, A. Clements, J. W. Collins, E. Elinav, G. J. Larrouy-Maumus, J. S. Choudhary and G. Frankel, Citrobacter rodentium Subverts ATP Flux and Cholesterol Homeostasis in Intestinal Epithelial Cells In Vivo, *Cell Metab*, 2017, **26**, 738-752 e736.
13. M. Farthing, M. A. Salam, G. Lindberg, P. Dite, I. Khalif, E. Salazar-Lindo, B. S. Ramakrishna, K. L. Goh, A. Thomson, A. G. Khan, J. Krabshuis, A. LeMair and Wgo, Acute diarrhea in adults and children: a global perspective, *J Clin Gastroenterol*, 2013, **47**, 12-20.
14. C. Lim, E. Takahashi, M. Hongsuwan, V. Wuthiekanun, V. Thamlikitkul, S. Hinjoy, N. P. Day, S. J. Peacock and D. Limmathurotsakul, Epidemiology and burden of multidrug-resistant bacterial infection in a developing country, *Elife*, 2016, **5**.
15. D. Stan, A. M. Enciu, A. L. Mateescu, A. C. Ion, A. C. Brezeanu, D. Stan and C. Tanase, Natural Compounds With Antimicrobial and Antiviral Effect and Nanocarriers Used for Their Transportation, *Front Pharmacol*, 2021, **12**, 723233.
16. R. Mattioli, A. Francioso, L. Mosca and P. Silva, Anthocyanins: A Comprehensive Review of Their Chemical Properties and Health Effects on Cardiovascular and Neurodegenerative Diseases, *Molecules*, 2020, **25**.
17. W. Y. Huang, Y. M. Liu, J. Wang, X. N. Wang and C. Y. Li, Anti-inflammatory effect of the blueberry anthocyanins malvidin-3-glucoside and malvidin-3-galactoside in endothelial cells, *Molecules*, 2014, **19**, 12827-12841.
18. D. D. Herrera-Balandrano, Z. Chai, R. P. Hutabarat, T. Beta, J. Feng, K. Ma, D. Li and W. Huang, Hypoglycemic and hypolipidemic effects of blueberry anthocyanins by AMPK activation: In vitro and in vivo studies, *Redox Biol*, 2021, **46**, 102100.
19. F. Liu, T. T. Y. Wang, Q. Tang, C. Xue, R. W. Li and V. C. H. Wu, Malvidin 3-Glucoside Modulated Gut Microbial Dysbiosis and Global Metabolome Disrupted in a Murine Colitis Model Induced by Dextran Sulfate Sodium, *Mol Nutr Food Res*, 2019, **63**, e1900455.
20. S. Talavera, C. Felgines, O. Texier, C. Besson, C. Manach, J. L. Lamaison and C. Remesy, Anthocyanins are efficiently absorbed from the small intestine in rats, *J Nutr*, 2004, **134**, 2275-2279.
21. M. Hidalgo, M. J. Oruna-Concha, S. Kolida, G. E. Walton, S. Kallithraka, J. P. Spencer and S. de Pascual-Teresa, Metabolism of anthocyanins by human gut microflora and their influence on gut bacterial growth, *J Agric Food Chem*, 2012, **60**, 3882-3890.
22. A. D. Smith, S. Botero, T. Shea-Donohue and J. F. Urban, Jr., The pathogenicity of an enteric Citrobacter rodentium Infection is enhanced by deficiencies in the antioxidants selenium and vitamin E, *Infect Immun*, 2011, **79**, 1471-1478.
23. A. D. Smith, N. S. George, L. Cheung, G. V. Bhagavathy, D. L. Luthria, K. M. John and A. A. Bhagwat, Pomegranate peel extract reduced colonic damage and bacterial translocation in a mouse model of infectious colitis induced by Citrobacter rodentium, *Nutr Res*, 2020, **73**, 27-37.
24. F. Liu, A. D. Smith, G. Solano-Aguilar, T. T. Y. Wang, Q. Pham, E. Beshah, Q. Tang, J. F. Urban, Jr., C. Xue and R. W. Li, Mechanistic insights into the attenuation of intestinal inflammation and modulation of the gut microbiome by krill oil using in vitro and in vivo models, *Microbiome*, 2020, **8**, 83.
25. E. Bolyen, J. R. Rideout, M. R. Dillon, N. A. Bokulich, C. C. Abnet, G. A. Al-Ghalith, H. Alexander, E. J. Alm, M. Arumugam, F. Asnicar, Y. Bai, J. E. Bisanz, K. Bittinger, A. Brejnrod, C. J. Brislawn, C. T. Brown, B. J. Callahan, A. M. Caraballo-Rodriguez, J. Chase, E. K. Cope, R. Da Silva, C. Diener, P. C. Dorrestein, G. M. Douglas, D. M. Durall, C. Duvallet, C. F. Edwardson, M. Ernst, M. Estaki, J. Fouquier, J. M. Gauglitz, S. M. Gibbons, D. L. Gibson, A. Gonzalez, K. Gorlick, J. Guo, B. Hillmann, S. Holmes, H. Holste, C. Huttenhower, G. A. Huttley, S. Janssen, A. K. Jarmusch, L. Jiang, B. D. Kaehler, K. B. Kang, C.

R. Keefe, P. Keim, S. T. Kelley, D. Knights, I. Koester, T. Kosciolek, J. Kreps, M. G. I. Langille, J. Lee, R. Ley, Y. X. Liu, E. Loftfield, C. Lozupone, M. Maher, C. Marotz, B. D. Martin, D. McDonald, L. J. McIver, A. V. Melnik, J. L. Metcalf, S. C. Morgan, J. T. Morton, A. T. Naimey, J. A. Navas-Molina, L. F. Nothias, S. B. Orchanian, T. Pearson, S. L. Peoples, D. Petras, M. L. Preuss, E. Pruesse, L. B. Rasmussen, A. Rivers, M. S. Robeson, 2nd, P. Rosenthal, N. Segata, M. Shaffer, A. Shiffer, R. Sinha, S. J. Song, J. R. Spear, A. D. Swafford, L. R. Thompson, P. J. Torres, P. Trinh, A. Tripathi, P. J. Turnbaugh, S. Ul-Hasan, J. J. J. van der Hooft, F. Vargas, Y. Vazquez-Baeza, E. Vogtmann, M. von Hippel, W. Walters, Y. Wan, M. Wang, J. Warren, K. C. Weber, C. H. D. Williamson, A. D. Willis, Z. Z. Xu, J. R. Zaneveld, Y. Zhang, Q. Zhu, R. Knight and J. G. Caporaso, Reproducible, interactive, scalable and extensible microbiome data science using QIIME 2, *Nat Biotechnol*, 2019, **37**, 852-857.

26. A. D. Fernandes, J. N. Reid, J. M. Macklaim, T. A. McMurrough, D. R. Edgell and G. B. Gloor, Unifying the analysis of high-throughput sequencing datasets: characterizing RNA-seq, 16S rRNA gene sequencing and selective growth experiments by compositional data analysis, *Microbiome*, 2014, **2**, 15.
27. N. Segata, J. Izard, L. Waldron, D. Gevers, L. Miropolsky, W. S. Garrett and C. Huttenhower, Metagenomic biomarker discovery and explanation, *Genome Biol*, 2011, **12**, R60.
28. J. Friedman and E. J. Alm, Inferring correlation networks from genomic survey data, *PLoS Comput Biol*, 2012, **8**, e1002687.
29. G. Yu, C. Xu, D. Zhang, F. Ju and Y. Ni, MetOrigin: Discriminating the origins of microbial metabolites for integrative analysis of the gut microbiome and metabolome, 2022, **1**, e10.
30. W. Li, R. A. Richter, Y. Jung, Q. Zhu and R. W. Li, Web-based bioinformatics workflows for end-to-end RNA-seq data computation and analysis in agricultural animal species, *BMC Genomics*, 2016, **17**, 761.
31. V. K. Mootha, C. M. Lindgren, K. F. Eriksson, A. Subramanian, S. Sihag, J. Lehar, P. Puigserver, E. Carlsson, M. Ridderstrale, E. Laurila, N. Houstis, M. J. Daly, N. Patterson, J. P. Mesirov, T. R. Golub, P. Tamayo, B. Spiegelman, E. S. Lander, J. N. Hirschhorn, D. Altshuler and L. C. Groop, PGC-1alpha-responsive genes involved in oxidative phosphorylation are coordinately downregulated in human diabetes, *Nat Genet*, 2003, **34**, 267-273.
32. Y. Yang, Wnt signaling in development and disease, *Cell Biosci*, 2012, **2**, 14.
33. H. E. Khoo, A. Azlan, S. T. Tang and S. M. Lim, Anthocyanidins and anthocyanins: colored pigments as food, pharmaceutical ingredients, and the potential health benefits, *Food Nutr Res*, 2017, **61**, 1361779.
34. D. Burdulis, A. Sarkinas, I. Jasutiene, E. Stackevicene, L. Nikolajevas and V. Janulis, Comparative study of anthocyanin composition, antimicrobial and antioxidant activity in bilberry (Vaccinium myrtillus L.) and blueberry (Vaccinium corymbosum L.) fruits, *Acta Pol Pharm*, 2009, **66**, 399-408.
35. K. A. Youdim, J. McDonald, W. Kalt and J. A. Joseph, Potential role of dietary flavonoids in reducing microvascular endothelium vulnerability to oxidative and inflammatory insults (small star, filled), *J Nutr Biochem*, 2002, **13**, 282-288.
36. N. O. Eltai, A. A. Al Thani, S. H. Al Hadidi, K. Al Ansari and H. M. Yassine, Antibiotic resistance and virulence patterns of pathogenic Escherichia coli strains associated with acute gastroenteritis among children in Qatar, *BMC Microbiol*, 2020, **20**, 54.
37. T. J. Ochoa and C. A. Contreras, Enteropathogenic escherichia coli infection in children, *Curr Opin Infect Dis*, 2011, **24**, 478-483.
38. C. Mullineaux-Sanders, J. Sanchez-Garrido, E. G. D. Hopkins, A. R. Shenoy, R. Barry and G. Frankel, Citrobacter rodentium-host-microbiota interactions: immunity, bioenergetics and metabolism, *Nat Rev Microbiol*, 2019, **17**, 701-715.
39. H. T. Hop, A. W. B. Reyes, T. X. N. Huy, L. T. Arayan, W. Min, H. J. Lee, M. H. Rhee, H. H. Chang and S. Kim, Activation of NF-kB-Mediated TNF-Induced Antimicrobial Immunity Is Required for the Efficient Brucella abortus Clearance in RAW 264.7 Cells, *Front Cell Infect Microbiol*, 2017, **7**, 437.
40. L. Tortola, R. Nitsch, M. J. M. Bertrand, M. Kogler, Y. Redouane, I. Kozieradzki, I. Uribesalgo, L. M. Fennell, M. Daugaard, H. Klug, G. Wirnsberger, R. Wimmer, T. Perlot, R. Sarao, S. Rao, T. Hanada, N. Takahashi, E. Kernbauer, D. Demiroz, M. Lang, G. Superti-Furga, T. Decker, A. Pichler, F. Ikeda, G. Kroemer, P. Vandenabeele, P. H. Sorensen and J. M. Penninger, The Tumor Suppressor Hace1 Is a Critical Regulator of TNFR1-Mediated Cell Fate, *Cell Rep*, 2016, **15**, 1481-1492.
41. C. Kucuk, X. Hu, J. Iqbal, P. Gaulard, D. Klinkebiel, A. Cornish, B. J. Dave and W. C. Chan, HACE1 is a tumor suppressor gene candidate in natural killer cell neoplasms, *Am J Pathol*, 2013, **182**, 49-55.
42. Y. G. Zhang, M. Singhal, Z. Lin, C. Manzella, A. Kumar, W. A. Alrefai, P. K. Dudeja, S. Saksena, J. Sun and R. K. Gill, Infection with enteric pathogens Salmonella typhimurium and Citrobacter rodentium modulate TGF-beta/Smad signaling pathways in the intestine, *Gut Microbes*, 2018, **9**, 326-337.

43. M. M. Shull, I. Ormsby, A. B. Kier, S. Pawlowski, R. J. Diebold, M. Yin, R. Allen, C. Sidman, G. Proetzel, D. Calvin and et al., Targeted disruption of the mouse transforming growth factor-beta 1 gene results in multifocal inflammatory disease, *Nature*, 1992, **359**, 693-699.
44. P. Leveen, J. Larsson, M. Ehinger, C. M. Cilio, M. Sundler, L. J. Sjostrand, R. Holmdahl and S. Karlsson, Induced disruption of the transforming growth factor beta type II receptor gene in mice causes a lethal inflammatory disorder that is transplantable, *Blood*, 2002, **100**, 560-568.
45. Y. Itatani, K. Kawada and Y. Sakai, Transforming Growth Factor-beta Signaling Pathway in Colorectal Cancer and Its Tumor Microenvironment, *Int J Mol Sci*, 2019, **20**.
46. C. Hoffmann, D. A. Hill, N. Minkah, T. Kirn, A. Troy, D. Artis and F. Bushman, Community-wide response of the gut microbiota to enteropathogenic Citrobacter rodentium infection revealed by deep sequencing, *Infect Immun*, 2009, **77**, 4668-4678.
47. A. Faria, I. Fernandes, S. Norberto, N. Mateus and C. Calhau, Interplay between anthocyanins and gut microbiota, *J Agric Food Chem*, 2014, **62**, 6898-6902.
48. R. Nocerino, F. De Filippis, G. Cecere, A. Marino, M. Micillo, C. Di Scala, C. de Caro, A. Calignano, C. Bruno, L. Paparo, A. M. Iannicelli, L. Cosenza, Y. Maddalena, G. Della Gatta, S. Coppola, L. Carucci, D. Ercolini and R. Berni Canani, The therapeutic efficacy of Bifidobacterium animalis subsp. lactis BB-12((R)) in infant colic: A randomised, double blind, placebo-controlled trial, *Aliment Pharmacol Ther*, 2020, **51**, 110-120.
49. N. Wang, S. Wang, B. Xu, F. Liu, G. Huo and B. Li, Alleviation Effects of Bifidobacterium animalis subsp. lactis XLTG11 on Dextran Sulfate Sodium-Induced Colitis in Mice, *Microorganisms*, 2021, **9**.
50. A. Sheikhi, M. Shakerian, H. Giti, M. Baghaeifar, A. Jafarzadeh, V. Ghaed, M. R. Heibor, N. Baharifar, Z. Dadafarin and G. Bashirpour, Probiotic Yogurt Culture Bifidobacterium Animalis Subsp. Lactis BB-12 and Lactobacillus Acidophilus LA-5 Modulate the Cytokine Secretion by Peripheral Blood Mononuclear Cells from Patients with Ulcerative Colitis, *Drug Res (Stuttg)*, 2016, **66**, 300-305.
51. H. Yang, H. C. Mirsepasi-Lauridsen, C. Struve, J. M. Allaire, A. Sivignon, W. Vogl, E. S. Bosman, C. Ma, A. Fotovati, G. S. Reid, X. Li, A. M. Petersen, S. G. Gouin, N. Barnich, K. Jacobson, H. B. Yu, K. A. Krogfelt and B. A. Vallance, Ulcerative Colitis-associated E. coli pathobionts potentiate colitis in susceptible hosts, *Gut Microbes*, 2020, **12**, 1847976.
52. J. Jansma, F. Brinkman, S. van Hemert and S. El Aidy, Targeting the endocannabinoid system with microbial interventions to improve gut integrity, *Prog Neuropsychopharmacol Biol Psychiatry*, 2021, **106**, 110169.
53. M. Igarashi, K. Iwasa and K. Yoshikawa, Feeding regulation by oleoylethanolamide synthesized from dietary oleic acid, *Prostaglandins Leukot Essent Fatty Acids*, 2021, **165**, 102228.
54. A. Romano, R. Coccurello, G. Giacovazzo, G. Bedse, A. Moles and S. Gaetani, Oleoylethanolamide: a novel potential pharmacological alternative to cannabinoid antagonists for the control of appetite, *Biomed Res Int*, 2014, **2014**, 203425.
55. L. Payahoo, Y. Khajebishak, M. Asghari Jafarabadi and A. Ostadrahimi, Oleoylethanolamide Supplementation Reduces Inflammation and Oxidative Stress in Obese People: A Clinical Trial, *Adv Pharm Bull*, 2018, **8**, 479-487.
56. M. Di Paola, E. Bonechi, G. Provensi, A. Costa, G. Clarke, C. Ballerini, C. De Filippo and M. B. Passani, Oleoylethanolamide treatment affects gut microbiota composition and the expression of intestinal cytokines in Peyer's patches of mice, *Sci Rep*, 2018, **8**, 14881.
57. A. Vijay, A. Kouraki, S. Gohir, J. Turnbull, A. Kelly, V. Chapman, D. A. Barrett, W. J. Bulsiewicz and A. M. Valdes, The anti-inflammatory effect of bacterial short chain fatty acids is partially mediated by endocannabinoids, *Gut Microbes*, 2021, **13**, 1997559.
58. M. A. Karwad, D. G. Couch, K. L. Wright, C. Tufarelli, M. Larvin, J. Lund and S. E. O'Sullivan, Endocannabinoids and endocannabinoid-like compounds modulate hypoxia-induced permeability in CaCo-2 cells via CB1, TRPV1, and PPARalpha, *Biochem Pharmacol*, 2019, **168**, 465-472.
59. M. Igarashi, K. Watanabe, T. Tsuduki, I. Kimura and N. Kubota, NAPE-PLD controls OEA synthesis and fat absorption by regulating lipoprotein synthesis in an in vitro model of intestinal epithelial cells, *FASEB J*, 2019, **33**, 3167-3179.

Figure legends

Figure 1. Malvidin intake alleviated the colitis phenotypes induced by *Citrobacter rodentium* in mice. A: Bodyweight change during the experiment. B: *Citrobacter rodentium* bacterial load (log_{10} cfu per gram of the colon tissue). C: Colon crypt length (μm). D: The cross-section of the colon tissues. NC: uninfected mice supplemented with PBS. CM: *Citrobacter rodentium* infected mice supplemented with PBS. MG: *Citrobacter rodentium* infected mice supplemented with malvidin 3-glycoside at 4 mg/kg bodyweight/day for a total of 17 days. ** $p < 0.01$; *** $p < 0.001$.

Figure 2. Malvidin supplementation induced a significant change in the transcritpome of the mouse proximal colon tissue. A: Volcano plot of RNAseq data. The log_2 (FC) (fold change) is plotted on the x-axis, and the negative log_{10} p-value is plotted on the y-axis. B: An enrichment plot of significantly enriched TGF-beta signaling pathway by the GSEA algorithm. C: TNFα signaling via NFκB pathway was enriched among the genes significantly upregulated by malvidin 3-glucoside in the colon tissue. D - F: the normalized count data of genes signifivantly regulated by malvidin supplementation in the colon tissue. D: a gene encoding HECT domain E3 ligase 1 (Hace1). E: Lmbrd2; F: Arl13b. The y-axis: TPM: transcripts per million. NES: normalized enrichment score. FDR: false discovery rate. CM: *Citrobacter rodentium* infected mice supplemented with PBS. MG: *Citrobacter rodentium* infected mice supplemented with malvidin 3-glycoside at 4 mg/kg bodyweight/day. * $p < 0.05$; ** $p < 0.01$; *** $p < 0.001$.

Figure 3. Malvidin intake modulated gut microbial composition in *Citrobacter rodentium* infected mice. A: Constrained principal coordinates analysis plot (CPCoA) of Bray–Curtis distances constrained by the group. Each point corresponds to a different sample colored by the group. The percentage of variation indicated in each axis corresponds to the fraction of the total

variance explained. B: The cladogram obtained by the linear discriminant analysis effect size algorithm (LEfSe). C: The abundance of *Bifidobacterium animalis* was significantly increased by the malvidin supplementation. LDA: linear discriminant analysis score. D: The 15 most important features (taxa) discriminating the supplementation status (CM vs MG) identified by Random Forests classification model. NC: uninfected mice supplemented with PBS. CM: *Citrobacter rodentium* infected mice supplemented with PBS. MG: *Citrobacter rodentium* infected mice supplemented with malvidin 3-glycoside at 4 mg/kg bodyweight/day. N =10 per group.

Figure 4. Microbial asscoaition networks inferred using SparCC algorithm. The color of a node represents the phylum of this node that belongs to. The detailed interaction (positive or negative) between nodes in each network (NC, CM, and MG) was listed in the gray boxes. NC: uninfected mice supplemented with PBS. CM: *Citrobacter rodentium* infected mice supplemented with PBS. MG: *Citrobacter rodentium* infected mice supplemented with malvidin 3-glycoside at 4 mg/kg bodyweight/day.

Figure 5. Fecal metabolites and associated pathways dysregulated by *Citrobacter rodentium* infection in mice without malvidin supplementation. A: Metabolite origin-based metabolic pathway enrichment analysis (MPEA) identified the pathways significantly enriched in the metabolites dysregulated by *Citrobacter rodentium* infection. The y-axis: the origin of metabolites prediced by MetOrigin. The size of the circle represents the number of significantly dysregulated metabolites in each enriched pathway. The color denotes the significance of the enrichment (p value). B: Association networks between metabolites and gut microbiota features (taxa) in select pathways based on the origin of metabolites. Left: Pyrimidine metabolism (KEGG ko00240) with the metabolites of "Microbiota" origin. Right: Tryptophan metabolism (Ko00380) and D-alanine metabolism (ko00473) with the metabolites from shared origin of both host and microbiota (Co-metabolism). The node sign represents metabolites (diamonds) and microbial taxa (dots), respectively. The red/green color of nodes indicates up- (red) or down- (green) regulation. The line colors denotes positive (red) and negative (green) correlations between taxa and metabolites. C & D: The relationships between select metabolites and microbiota taxa for Kyoto Encyclopedia of Genes and Genomes (KEGG) pathways. Origin-

based metabolic function analysis and integrated visualization plots of two metabolic reactions in tryptophan metabolism using Sankey network algorithm: C: the metabolic reaction R02678; D: the metabolic reaction R02908. * denotes statistically significant correlations between a given taxon and a metabolite. The color of nodes indicates up- (red) or down-regulation (green). The red/green bands indicate the direction of the statistcial correlations (red = positive and green = negative) and the dark color represents the statistically significant correlations ($p < 0.05$).

Figure 6. Metabolic pathways significantly affected by malvidin 3-glycoside supplementation in *Citrobacter rodentium* infected mice. A: Fecal metabolite significantly affected by malvidin supplementation. X-axis: the $\log_2$ (FC) (fold change); Y-axis: negative $\log_{10}$ *p*-value. The dots represent individual metabolites positively annotated in the Human Metabolome Database. The arrow denotes the name of select metabolites significantly dysregulated. B: The relative level of three select metabolites, glutaric acid, indole, and pantothenic acid. C: The enriched metabolic pathways identified using origin-based metabolic pathway enrichment analysis. The dashed line represents the level of significance at adjusted $p = 0.05$. D: Predicted relationships among metabolites, metabolic pathways, and microbial taxa (genera) for the metabolites of "Microbiota" origin (left) and the origin shared by host and microbiota ("Co-metabolism", right). E: The detailed relationships between two select metabolites (indole) and L-tryptophan in metabolic reaction (R00673) belonging to tryptophan metabolism and microbiota features (taxa, from the phylum to genus levels). * $p < 0.05$.

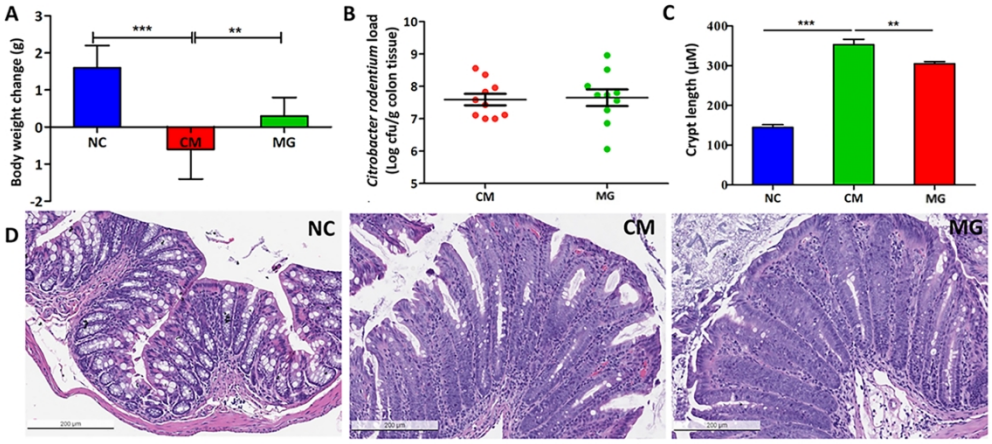

189x86mm (300 x 300 DPI)

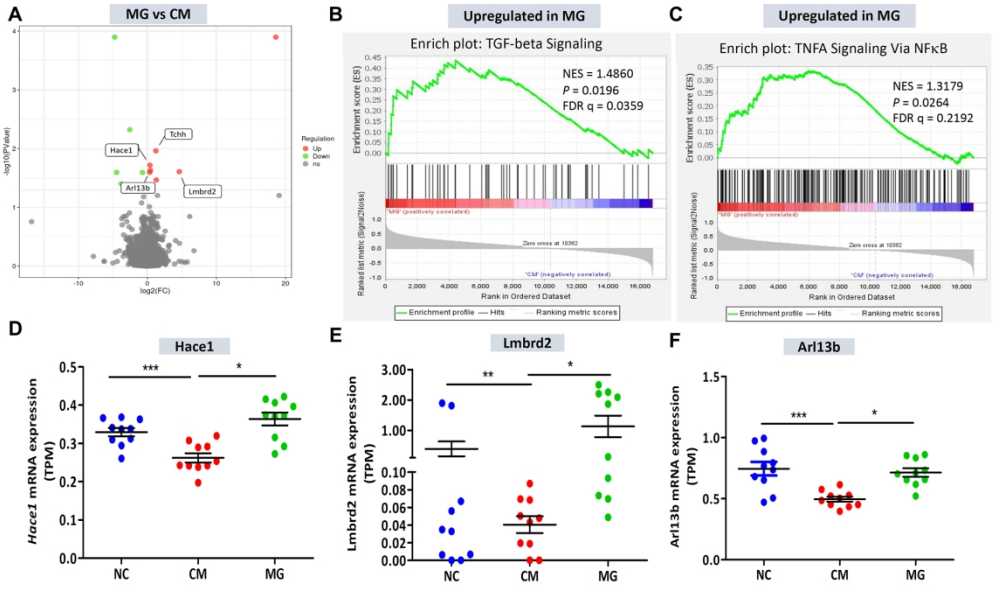

189x111mm (300 x 300 DPI)

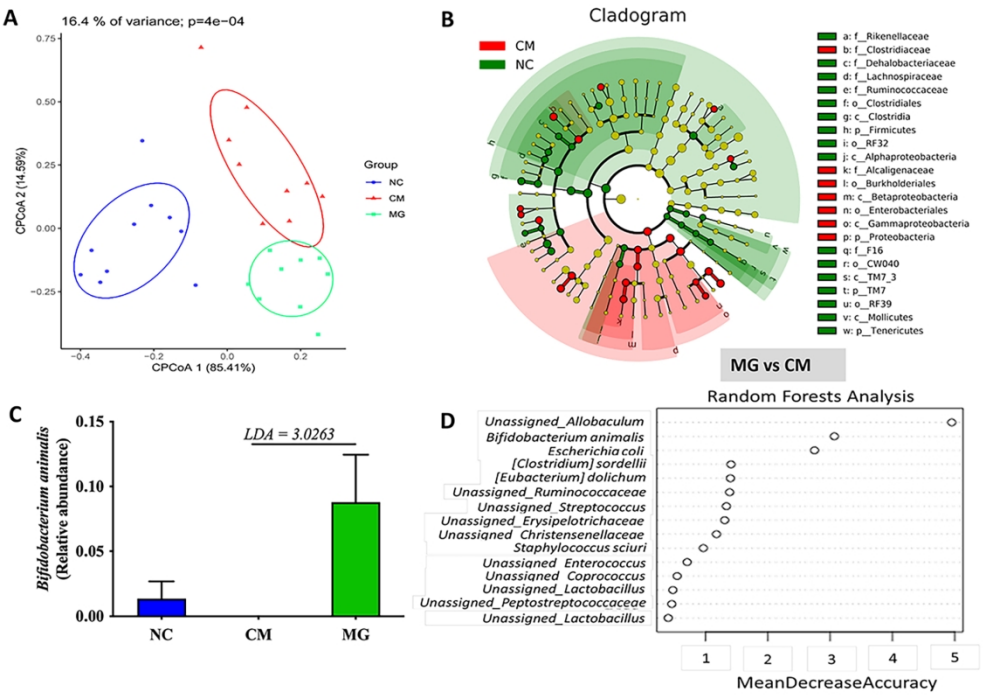

189x134mm (300 x 300 DPI)

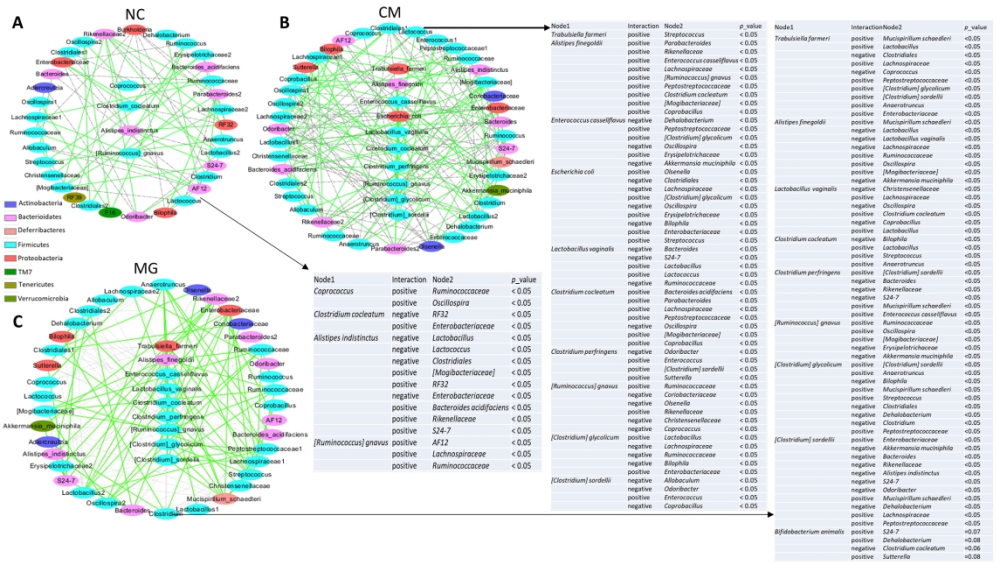

Node1	Interaction	Node2	p_value
Coprococcus	positive	*Ruminococcaceae*	< 0.05
	positive	*Oscillospira*	< 0.05
Clostridium cocleatum	negative	*RF32*	< 0.05
	positive	*Enterobacteriaceae*	< 0.05
Alistipes indistinctus	negative	*Lactobacillus*	< 0.05
	negative	*Lactococcus*	< 0.05
	negative	*Clostridiales*	< 0.05
	positive	*[Mogibacteriaceae]*	< 0.05
	positive	*RF32*	< 0.05
	negative	*Enterobacteriaceae*	< 0.05
	positive	*Bacteroides acidfaciens*	< 0.05
	positive	*Rikenellaceae*	< 0.05
	positive	*S24-7*	< 0.05
[Ruminococcus] gnavus	positive	*AF12*	< 0.05
	positive	*Lachnospiraceae*	< 0.05
	positive	*Ruminococcaceae*	< 0.05

Node1	Interaction	Node2	p_value
Trabusiella farmeri	positive	*Streptococcus*	< 0.05
Alistipes finegoldii	positive	*Parabacteroides*	< 0.05
	positive	*Rikenellaceae*	< 0.05
	positive	*Enterococcus casseliflavus*	< 0.05
	positive	*Lachnospiraceae*	< 0.05
	positive	*[Ruminococcus] gnavus*	< 0.05
	positive	*Peptostreptococcaceae*	< 0.05
	positive	*Clostridium cocleatum*	< 0.05
	positive	*[Mogibacteriaceae]*	< 0.05
	positive	*Coprobacillus*	< 0.05
Enterococcus casseliflavus	negative	*Dehalobacterium*	< 0.05
	positive	*Peptostreptococcaceae*	< 0.05
	positive	*[Clostridium] glycolicum*	< 0.05
	negative	*Oscillospira*	< 0.05
	positive	*Erysipelotrichaceae*	< 0.05
	negative	*Akkermansia muciniphila*	< 0.05
Escherichia coli	positive	*Olsenella*	< 0.05
	negative	*Clostridiales*	< 0.05
	negative	*Lachnospiraceae*	< 0.05
	positive	*[Clostridium] glycolicum*	< 0.05
	negative	*Oscillospira*	< 0.05
	positive	*Erysipelotrichaceae*	< 0.05
	negative	*Bilophila*	< 0.05
	positive	*Enterobacteriaceae*	< 0.05
	positive	*Streptococcus*	< 0.05
Lactobacillus vaginalis	negative	*Bacteroides*	< 0.05
	negative	*S24-7*	< 0.05
	positive	*Lactobacillus*	< 0.05
	positive	*Lactococcus*	< 0.05
	negative	*Ruminococcaceae*	< 0.05
Clostridium cocleatum	positive	*Bacteroides acidfaciens*	< 0.05
	positive	*Parabacteroides*	< 0.05
	positive	*Lachnospiraceae*	< 0.05
	positive	*Peptostreptococcaceae*	< 0.05
	negative	*Oscillospira*	< 0.05
	positive	*[Mogibacteriaceae]*	< 0.05
	positive	*Coprobacillus*	< 0.05
Clostridium perfringens	negative	*Odoribacter*	< 0.05
	positive	*Enterococcus*	< 0.05
	positive	*[Clostridium] sordellii*	< 0.05
	positive	*Sutterella*	< 0.05
[Ruminococcus] gnavus	positive	*Ruminococcaceae*	< 0.05
	negative	*Coriobacteriaceae*	< 0.05
	negative	*Olsenella*	< 0.05
	positive	*Rikenellaceae*	< 0.05
	negative	*Christensenellaceae*	< 0.05
	negative	*Coprococcus*	< 0.05
[Clostridium] glycolicum	positive	*Lactobacillus*	< 0.05
	negative	*Lachnospiraceae*	< 0.05
	negative	*Ruminococcaceae*	< 0.05
	negative	*Bilophila*	< 0.05
	positive	*Enterobacteriaceae*	< 0.05
[Clostridium] sordellii	negative	*Allobaculum*	< 0.05
	negative	*Odoribacter*	< 0.05
	positive	*Enterococcus*	< 0.05
	negative	*Coprobacillus*	< 0.05

Node1	Interaction	Node2	p_value
Trabusiella farmeri	positive	*Mucispirillum schaedleri*	<0.05
	positive	*Lactobacillus*	<0.05
	negative	*Clostridiales*	<0.05
	positive	*Lachnospiraceae*	<0.05
	negative	*Coprococcus*	<0.05
	positive	*Peptostreptococcaceae*	<0.05
	positive	*[Clostridium] glycolicum*	<0.05
	positive	*[Clostridium] sordellii*	<0.05
	positive	*Anaerotruncus*	<0.05
Alistipes finegoldii	positive	*Enterobacteriaceae*	<0.05
	positive	*Mucispirillum schaedleri*	<0.05
	negative	*Lactobacillus*	<0.05
	negative	*Lactobacillus vaginalis*	<0.05
	negative	*Lachnospiraceae*	<0.05
	negative	*Ruminococcaceae*	<0.05
	positive	*Oscillospira*	<0.05
	positive	*[Mogibacteriaceae]*	<0.05
Lactobacillus vaginalis	negative	*Christensenellaceae*	<0.05
	positive	*Lachnospiraceae*	<0.05
	negative	*Oscillospira*	<0.05
	positive	*Clostridium cocleatum*	<0.05
	negative	*Coprobacillus*	<0.05
	positive	*Lactobacillus*	<0.05
Clostridium cocleatum	negative	*Bilophila*	<0.05
	positive	*Lactobacillus*	<0.05
	positive	*Streptococcus*	<0.05
	positive	*Anaerotruncus*	<0.05
Clostridium perfringens	positive	*[Clostridium] sordellii*	<0.05
	negative	*Bacteroides*	<0.05
	negative	*Rikenellaceae*	<0.05
	negative	*S24-7*	<0.05
	positive	*Mucispirillum schaedleri*	<0.05
	positive	*Enterococcus casseliflavus*	<0.05
[Ruminococcus] gnavus	positive	*Ruminococcaceae*	<0.05
	positive	*Oscillospira*	<0.05
	positive	*[Mogibacteriaceae]*	<0.05
	negative	*Erysipelotrichaceae*	<0.05
	negative	*Akkermansia muciniphila*	<0.05
[Clostridium] glycolicum	positive	*[Clostridium] sordellii*	<0.05
	positive	*Anaerotruncus*	<0.05
	negative	*Bilophila*	<0.05
	positive	*Mucispirillum schaedleri*	<0.05
	positive	*Streptococcus*	<0.05
	negative	*Clostridiales*	<0.05
	negative	*Dehalobacterium*	<0.05
	negative	*Clostridium*	<0.05
	positive	*Peptostreptococcaceae*	<0.05
[Clostridium] sordellii	positive	*Enterobacteriaceae*	<0.05
	negative	*Akkermansia muciniphila*	<0.05
	negative	*Bacteroides*	<0.05
	negative	*Rikenellaceae*	<0.05
	negative	*Alistipes indistinctus*	<0.05
	negative	*S24-7*	<0.05
	negative	*Odoribacter*	<0.05
	positive	*Mucispirillum schaedleri*	<0.05
	negative	*Dehalobacterium*	<0.05
	positive	*Lachnospiraceae*	<0.05
	positive	*Peptostreptococcaceae*	<0.05
Bifidobacterium animalis	positive	*S24-7*	=0.07
	positive	*Dehalobacterium*	=0.08
	negative	*Clostridium cocleatum*	=0.06
	positive	*Sutterella*	=0.08

189x106mm (300 x 300 DPI)

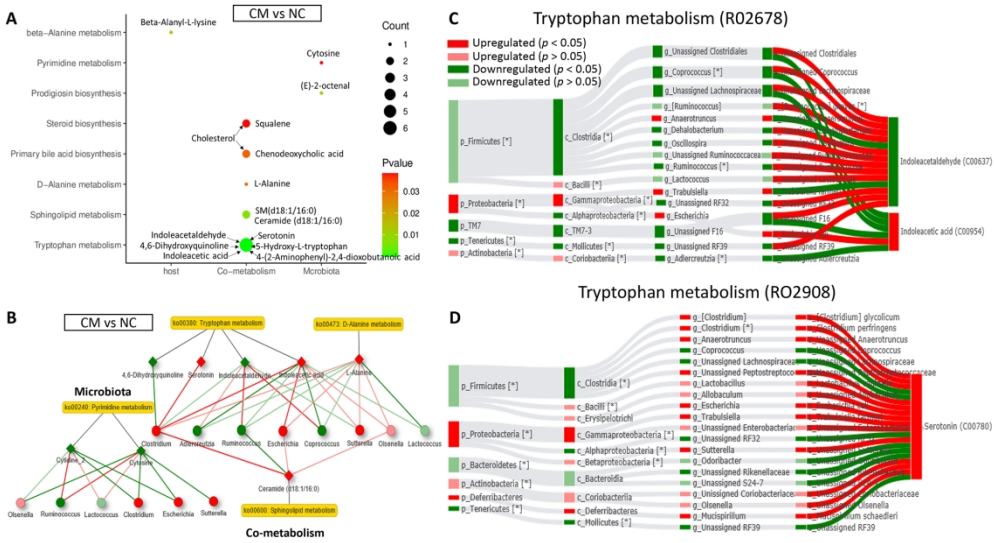

189x102mm (300 x 300 DPI)

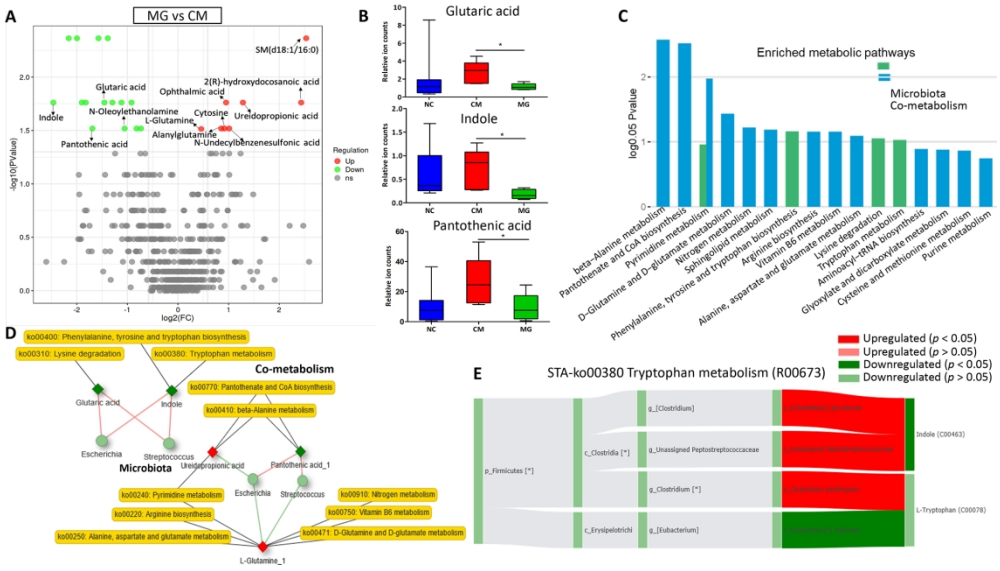

189x106mm (300 x 300 DPI)